3-2014

Diffuse Reflectance Spectroscopy of Epithelial Tissue with a Smart Fiber-optic Probe

Bing Yu
Marquette University, bing.yu@marquette.edu

Amy Shah
Vanderbilt University

Vivek K. Nagarajan
The University of Akron

Daron G. Ferris
Georgia Regents University

Biomedical Optics Express, Vol. 5, No. 3 (March 2014): 675-689. DOI.

Diffuse Reflectance Spectroscopy of Epithelial Tissue with a Smart Fiber-optic Probe

Bing Yu
Department of Biomedical Engineering, The University of Akron, Akron, OH
Amy Shah
Department of Biomedical Engineering, Vanderbilt University, Nashville, TN
Vivek K. Nagarajan
Department of Biomedical Engineering, The University of Akron, Akron, OH
Daron G. Ferris
Department of Family Medicine and Obstetrics and Gynecology, Georgia Regents University, Augusta, GA

Abstract

Diffuse reflectance spectroscopy (DRS) with a fiber-optic probe can noninvasively quantify the optical properties of epithelial tissues and has shown the potential as a cost-effective, fast and sensitive tool for diagnosis of early precancerous changes in the cervix and oral cavity. However, current DRS systems are susceptible to several sources of systematic and random errors, such as uncontrolled probe-to-tissue pressure and lack of a real-time

calibration that can significantly impair the measurement accuracy, reliability and validity of this technology as well as its clinical utility. In addition, such systems use bulky, high power and expensive optical components which impede their widespread use in low- and middle-income countries (LMICs) where epithelial cancer related death is disproportionately high. In this paper we report a portable, easy-to-use and low cost, yet accurate and reliable DRS device that can aid in the screening and diagnosis of oral and cervical cancer. The device uses an innovative smart fiber-optic probe to eliminate operator bias, state-of-the-art photonics components to reduce size and power consumption, and automated software to reduce the need of operator training. The device showed a mean error of 1.4 ± 0.5% and 6.8 ± 1.7% for extraction of phantom absorption and reduced scattering coefficients, respectively. A clinical study on healthy volunteers indicated that a pressure below 1.0 psi is desired for oral mucosal tissues to minimize the probe effects on tissue physiology and morphology.

1. Introduction

Numerous studies have shown that epithelial cancers, such as oral and cervical cancers, if detected at early stages, have a better chance of being successfully treated with surgery, radiation, chemotherapy, or a combination of the three, therefore significantly improving the survival rates [1–8]. Detecting and grading precancerous and malignant oral lesions is mostly accomplished by visual screening and biopsy of suspicious tissue sites. The Pap smear is the standard of care for screening for cervical cancer. An effective cancer screening and diagnostic program often requires both sophisticated and expensive medical facilities and well-trained doctors and nurses. In developing countries epithelial cancer related death is disproportionately high due to the absence of appropriate medical infrastructure and resources to support the organized screening and diagnostic programs that are available in the developed world.

DRS in the visible wavelength range is sensitive to the absorption and scattering properties of epithelial tissue and has shown promise for early diagnosis of cancers in the cervix and oral cavity [9–24]. The absorption and scattering coefficients of epithelial tissues reflect their underlying physiological and morphological properties [25]. In the visible band, dominant absorbers in oral and cervical tissue are oxygenated (HbO_2) and deoxygenated hemoglobin (Hb), arising from blood vessels in the stroma. Light scattering is primarily caused by cell nuclei and organelles in the epithelium and stroma, as well as collagen fibers and cross-links in stroma. Neoplastic tissue exhibit significant changes in their physiological and morphological characteristics that can be quantified optically: Stromal layer absorption is expected to increase with angiogenesis, whereas stromal scattering is expected to go down with neoplastic progression as extracellular collagen networks degrade [11, 25–29]. Epithelial scattering has been shown to increase due to increased nuclear size, increased DNA content, and hyperchromasia [25–27, 30]. Visible DRS has a penetration depth that can be tuned to be comparable to the thickness of the epithelial layer or deeper to probe both the epithelial and stromal layers [17, 25, 31].

Zhu et al. [32] have developed a UV-VIS DRS system with a probe geometry that is most sensitive to changes in epithelium and stroma. Palmer et al [33] have developed a scalable inverse Monte Carlo (MC) model to rapidly measure and quantify tissue optical properties. Chang et al [10] used the system and MC model to identify contrasts in optical biomarkers that vary with different grades of cervical intraepithelial neoplasia (CIN) from normal cervical tissues from 38 patients. Total hemoglobin (THb) was found to be statistically higher in high grade CIN compared with normal and low grade CIN, whereas scattering was significantly reduced in CIN compared with normal tissues. In a study of a hamster cheek pouch model of oral carcinogenesis Skala et al. [9] found that the scattering was significantly lower in neoplastic samples than in normal samples. These findings are also consistent with those reported by Wang, et al. [25], Arifler et al. [26], and Georgakoudi, et al. [30].

Current DRS systems typically consist of a broadband source, a spectrometer for multi-spectral detection and a fiber-optic probe for relaying light to and from the instrument [34]. However, these systems have not been

specifically designed to be robust and reliable, especially in LMICs. Potential sources of systematic or random errors can arise from the uncontrolled probe-tissue interface and the lack of robust, real-time calibration technique. First, uncontrolled probe-to-tissue coupling and pressure can make it difficult to obtain a reproducible and intact tissue reflectance spectrum. Chan et al found that there was a decrease in the diffuse reflectance and increase in the scattering coefficient between 400 and 1800 nm with compression of *in vitro* human skin [35]. Reif et al. reported a study in which reflectance measurements were obtained *in vivo* from mouse thigh muscles while varying the contact pressure of the fiber-optic probe [36]. They found that the extracted blood vessel radius, oxygen saturation, and Mie theory slope decreased with pressure, while the reduced scattering coefficient at 700 nm increased as a function of pressure. Recently, Ti and Lin studied the short- and long-term effects of probe pressure on *in vivo* diffuse reflectance using an animal model [37]. They concluded that elevation in probe pressure can induce major alterations in the profile of the reflectance spectra between 400 and 650 nm and the changes in the extracted tissue optical properties depend not only on the probe pressure, but also on tissue type. Similar findings have also been reported by Nath et al. [38], Rivoire et al. [39], Shangguan at al [40], Atencio at al., [41] Chen, et al. [42], and Ruderman at al. [43]. It is generally believed that the changes may be attributed to the compression of the blood vessels which causes reduced blood flow and alterations in the metabolism of the tissue as well as a change in the density of the scatterers. It is therefore critical to measure and control the probe contact pressure in order to obtain reproducible and intact tissue physiological parameters.

Recently, Kienle at al., [44] remotely measured spatially resolved absolute diffuse reflectance of biological tissue with a laser source and a CCD camera. Gebhart et al. [45], described a noncontact diffuse reflectance imaging system using a liquid-crystal tunable filter for brain tumor demarcation. Bish et al. [46], developed a diffuse optical spectroscopy probe that images the illumination and collection fibers onto the tissue surface for measuring tissue optical properties. More recently, Cuccia et al. [47], employed structured illumination imaging for mapping of tissue optical properties. All these noncontact imaging approaches can avoid the effect of probe-tissue pressure and have a large field-of-view with high spatial resolution. The major drawbacks of noncontact imaging setups, compared with fiber probe based DRS, include the need of expensive and bulky tunable light sources and CCD cameras; the lack of a well-defined sensing depth; and the challenges to access deep tissue sites or internal organs.

Second, the lack of a robust, real-time calibration technique makes the calibration process time-consuming and potentially inaccurate, particularly when attempting to quantify absolute absorption and scattering coefficients. To consistently yield accurate estimation of tissue optical properties, calibration is required to compensate for the wavelength-dependent instrument response, lamp intensity fluctuations, and fiber bending losses [48, 49]. Current calibration techniques typically rely on measurements using reflectance standards and/or tissue phantoms after the clinical measurements are completed [18, 33, 50–52]. There are a number of limitations associated with such calibration methods. First, because the calibration is performed at the beginning or end of the study, real-time instrument fluctuations, such as lamp drift and fiber bending loss cannot be compensated by these approaches. Second, they may require an additional 30 minutes for lamp warm-up and another 10-20 minutes for calibration, which is a significant amount of time in a clinical setting.

Finally, most DRS systems use thermal light sources, grating spectrographs, and cooled CCD cameras. Thermal light sources have large footprint, short life-time, low power efficiency, and low coupling efficiency to optical fibers. Spectrometers using grating spectrographs and cooled CCD cameras have extremely high wavelength resolution and sensitivity, but are very bulky and expensive and consume a large amount of electrical power. In addition, a stable power supply is very often required to operate a thermal lamp and a CCD camera. The system complexity also makes it necessary for the operator to have extensive knowledge in optical spectroscopy and

professional training on the instrument and probes. Taken together, it is very difficult for DRS systems in their current forms to be directly used for cancer screening in resource limited settings.

Yu et al. previously reported a self-calibrating (SC) probe based-on a traditional spectrometer for performing visible DRS [53, 54] and the clinical test of the technology with a portable system for cervical cancer screening in Haiti [55]. The results demonstrated that a built-in SC channel in the fiber-optic probe can be used to correct for the effects of fluctuations in the DRS intensity due to light source drifts and fiber-bending attenuation, thus significantly improves the accuracy in measuring tissue scattering coefficients. The clinical study in Haiti also indicated that without a pressure senor, the probe pressure could vary up to 3-5 psi (data not included in the paper). Yu et al. has previously demonstrated a diaphragm-based fiber-optic interferometric (DFPI) pressure sensor for on-line detection of acoustic waves generated from partial discharges (PDs) in high power transformers [56] and dynamic pressure monitoring in jet turbine engines [57, 58]. The DFPI sensors showed a sensitivity of 87 mV/psi and a high resolution of 0.023 psi (or 159 Pa) and a dynamic range over 100 psi [57, 58].

In this report, we describe a smart fiber-optic probe based on a portable DRS instrument that extends the capability of the SC probe by integrating a DFPI pressure sensor with the self-calibration probe to eliminate operator bias and to reduce size and power consumption as well as the need of operator training. The pressure sensor provides real-time feedback on the probe pressure so that the operator can manually adjust the force applied on it. If and only if the measured probe falls within a preset range the DRS tissue and SC spectra are analyzed. Test results from phantom and volunteer studies are presented to demonstrate the capability of the device as well as how oral mucosa responds to probe pressure.

2. Method and materials

2.1. Instrumentation

Figure 1(a) shows a schematic of the main components of the smart fiber-optic probe and the instrument to which it is coupled. The probe integrates a tissue sensing channel, a SC channel [53, 54], and a DFPI pressure sensor [59] into a single fiber-optic probe. The instrument consists of an 850 nm LED (A2000, Appointech Inc., Taiwan), a high power white LED (LEDC1-W55, Doric Lenses Inc., Quebec, Canada), a three-channel fiber-optic USB spectrometer (AvaSpec-2048, Avantes BV, The Netherlands), and a laptop with custom LabVIEW (National Instruments Corp., TX) and Matlab (Mathworks Inc., MA) software. The sensing and calibration channels share the white LED as the light source, while the pressure sensor uses the 850 nm LED as its light source. The USB spectrometer includes two visible channels (Spec A & B), covering a wavelength range from 400 - 635 nm with a wavelength resolution of 1.8 nm, for detection of the tissue DRS and SC spectra, respectively. The NIR spectrometer (Spec C) has a wavelength coverage from 750 to 932 nm with 0.23 nm resolution and is used for detection of the interferograms from the DFPI pressure sensor. A better wavelength resolution is required for the NIR channel to resolve the sharp interferograms of the DFPI sensor.

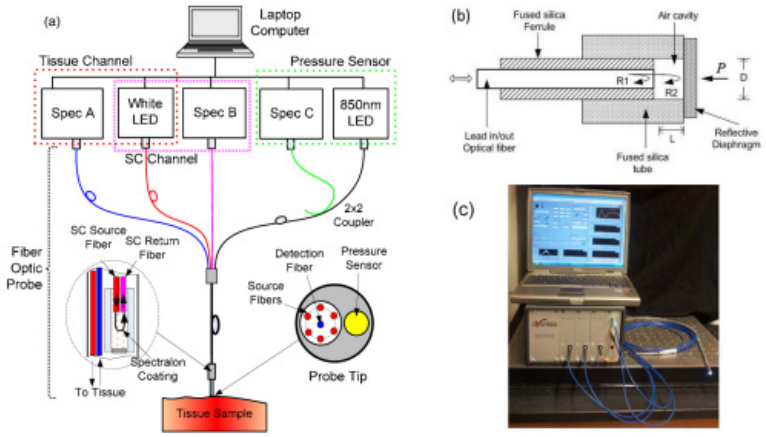

Fig. 1 A smart optic sensor system: (a) schematic of the probe and instrument; (b) schematic of the DFPI pressure sensor head; and (c) photograph of the portable instrument and smart probe. LED – light emitting diode; Spec – spectrometer; R_1 and R_2 – reflection; P – external pressure; and D – diameter of the glass diaphragm.

At the distal end, the tissue channel uses a single fiber (the blue fiber) for DRS detection (connected to Spec A) and six source fibers (the red fibers) forming a ring around the detection fiber for tissue illumination. For oral mucosal tissue, a source-detector separation (the radius of the illumination ring) of 640 µm was used, which provides a simulated sensing depth of 0.5-2 mm. The SC source fiber (one of the seven red fibers from the white LED) is looped back, by the 99% Spectralon diffuse reflectance coating (Labsphere Inc, North Sutton, NH) inside the rigid part of the probe housing, into a SC detection fiber (the pink fiber) that is connected to the Spec B. All fibers for the tissue and SC channels use the same type of 200/220-µm fiber with a numerical aperture (NA) of 0.22. Six inches of the fiber-optic cable immediately after the rigid probe tip was mounted inside a gooseneck tube so that the probe can be easily bent to different angles inside an oral cavity. The center to center distance between the pressure sensor and source-detection fiber ring is 3.1 mm. The diameter of the entire probe tip is 6.5 mm. Since the probe tip is flat with edge slightly rounded, the variation in the pressure across the probe tip should be very small.

The principle of the DFPI pressure sensor was described in detail in Reference [56] and is briefly restated here. The broadband NIR light from the 850 nm LED is launched into a DFPI sensor through a 2 × 2 fiber-optic coupler whose other input leg (the green fiber) is connected to Spec C. The tip of the unused output leg is immersed in index matching gel to minimize unnecessary back reflection. All fibers used in the NIR channel are 50/125-µm multimode fibers. The DFPI sensor head, as shown in Fig. 1(b), is basically a low-coherence Fabry-Perot interferometer (FPI) formed by the cleaved end face of the lead in/out fiber and the inner surface of a glass diaphragm. The optical fiber, fused silica ferrule and tube, as well as the diaphragm are bonded together using high temperature epoxy. The reflected lights from the two air-glass interfaces (R_1 and R_2) propagate back to Spec C, generating interference fringes (or interferogram). External pressure *P* applied on the outer surface of the diaphragm deflects it towards the fiber tip, thus reduce the cavity length of the DFPI and cause a shift in the peak positions and a reduction in the fringe density of the interferogram on Spec C. By analyzing the interferogram using a simple fringe peak tracking algorithm [60], the cavity length, and thus applied pressure can be determined. A probe pressure range of 0–8 psi is selected according to literature for similar studies [36, 37, 40].

2.2. Software

A LabVIEW program was developed to automate the data collection and analysis processes so that minimum training is required to operate the instrument. A flowchart of the program is shown in Fig. 2. The LabVIEW

software includes the following function modules: (1) initializing the spectrometers, selecting the probe and target type (phantom or tissue subject), and loading saved probe configuration information; (2) acquiring phantom/tissue, calibration and pressure spectra; (3) calling the interferogram analysis algorithm in Matlab to calculate the probe pressure P from the NIR spectrum; (4) performing self-calibration; (5) calling a Monte Carlo inversion model in Matlab to analyze the tissue spectrum if the pressure is within the preset range; and (6) displaying the raw spectra as well as calculated probe pressure and extracted tissue parameters, such as the hemoglobin concentrations (HbO_2, Hb and THb), oxygen saturation (SO_2), and wavelength averaged reduced scattering coefficient ($\mu_s' < \lambda >$). The time required to measure and analyze the spectra from a tissue sample is approximately 1-2 seconds.

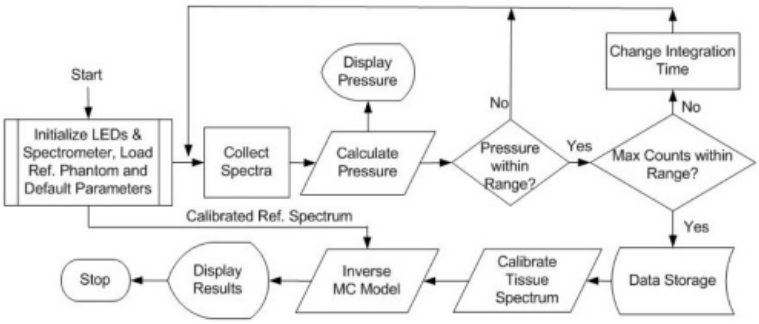

Fig. 2 Flowchart of the LabVIEW software for instrument control and data collection and analysis.

2.3. Instrument and probe characterization

2.3.1. Phantom validation of the tissue and SC channels

A phantom study was performed to evaluate the performance of the constructed smart sensor system in measuring tissue optical properties. The phantoms contained variable concentrations of hemoglobin (H0267, Sigma-Aldrich Co. LLC) as the absorber and 1-µm polystyrene microspheres (07310-15, Polysciences Inc.) as the scatterer. 14 phantoms covering a hemoglobin concentration range of 4-33.6 µM in water were created by fixing the number of scatterers and titrating the absorber. The absorption coefficient ($\mu_a(\lambda)$) was independently determined from a spectrophotometer (Lambda 35, PerkinElmer Inc.) measurement of a diluted hemoglobin stock solution and the reduced scattering coefficients ($\mu_s'(\lambda)$) was calculated using the Mie theory for known size, density and refractive index of the scatterers. Table 1 summarizes the phantom hemoglobin concentration and expected mean $< \mu_a(\lambda) >$ and $< \mu_s'(\lambda) >$ between the wavelength range of 430-630 nm.

Table 1. Summary of phantom THb and expected mean optical properties between 430 and 630 nm.

Phantom #	THb (µM)	Expected $< \mu_s'(\lambda) >$ cm^{-1}	Expected $< \mu_a(\lambda) >$ cm^{-1}
1	4.00	12.97	0.33
2	7.61	12.34	0.64
3	10.88	11.77	0.91
4	13.86	11.24	1.16
5	16.59	10.77	1.39
6	19.10	10.33	1.60
7	21.41	9.92	1.79
8	23.54	9.55	1.97
9	25.52	9.20	2.14
10	27.36	8.88	2.29

11	29.08	8.58	2.43
12	30.68	8.30	2.57
13	32.19	8.03	2.69
14	33.60	7.79	2.81

A full diffuse reflectance spectrum (400-635nm) was measured with a calibration spectrum concurrently from each phantom using the smart sensor system and smart probes. The calibration was performed by dividing the phantom spectrum by the calibration spectrum (point-by-point). A Monte Carlo inverse model of reflectance [33] was used to extract the phantom $\mu_a(\lambda)$ and $\mu_s'(\lambda)$ as well as THb concentration (100% HbO_2) from the self-calibrated phantom spectrum between 430 and 630 nm, following the procedures described by Yu et al. [54] Next, the percent errors, which are the difference between the absolute value of the extracted and expected values in $< \mu_a(\lambda) >$ and $< \mu_s'(\lambda) >$, were computed.

2.3.2. Pressure sensor characterization

The pressure response of the smart sensor was characterized in a pressure test setup, as shown in Fig. 3. The probe tip was mounted and sealed into the test tube through a fitting. The pressure was provided by a gas cylinder with compressed nitrogen through a gas pipe. The pressure was controlled by adjusting the pressure regulator on the cylinder and the accurate pressure was monitored by a digital pressure gauge (DPG1000AD-30G, OMEGA Engineering, Inc.). The gauge has a resolution of 0.1 psi within 0-30 psi. During the experiment, the gas pressure inside the tube was increased from 0 psi (atmospheric pressure) to 8 psi, at a step of 1.0 psi. At each pressure level, 10 repeated measurements were taken. The measured air cavity length (L) of the DFPI sensor was plotted against the applied nitrogen pressure (P) and the L-P curve was used to calculate the sensitivity of the sensor and calibrate the pressure sensor.

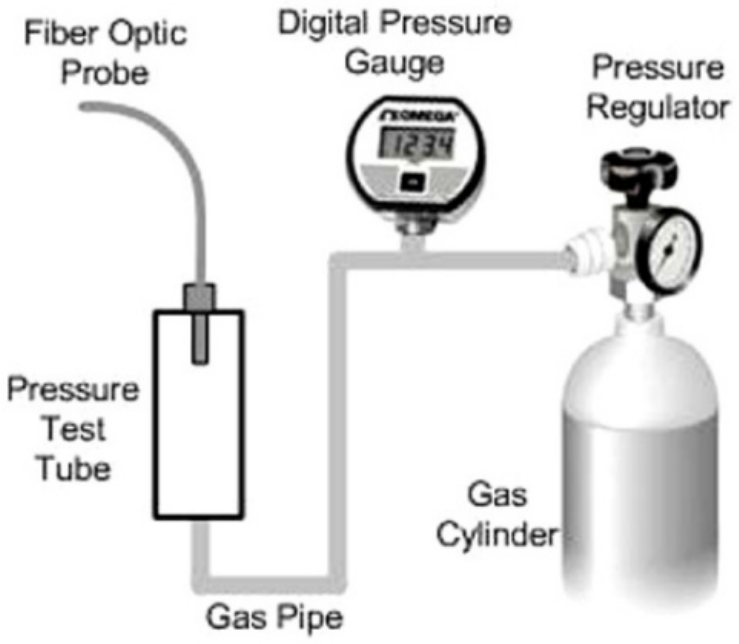

Fig. 3 Schematic of experimental setup for pressure sensor test.

2.4. Volunteer studies

To find out how well the probe pressure on an *in vivo* tissue sample can be controlled with the smart sensor and how oral mucosal tissues respond to probe pressure, DRS measurements have been taken from a total of 8 healthy volunteers. The study has been approved by the Institutional Review Boards at both Duke University and The University of Akron. Informed consent has been obtained from each study subject prior to the DRS measurements.

2.4.1. Pressure control

DRS measurements have been taken from an *in vivo* tissue sample with constant probe pressure to estimate how well the probe pressure can be controlled with the smart sensor. During the experiment, the probe was brought in contact with a volunteer's finger (Vol 1) and the preset probe pressure was set between 2 and 3 psi and best effort was taken to maintain the pressure within this range. A total of 170 pressure measurements have been taken within ~200 seconds. The actual probe pressure has been recorded at each scan and analyzed.

2.4.2. Tissue response to pressure

A. Variable probe pressure

To evaluate the response of oral mucosa to probe pressure, a total of 7 volunteers (Vol 2-8) were measured with the smart sensor. Before the optical measurements, all volunteers were asked to rinse their mouth with a 0.9% saline solution in order to minimize the influence of consumed food. The probe was cleaned using 2% chlorhexidine digluconate in ethanol. The probe was then placed in contact with the mucosal tissue from the inner surface of the left cheek of each volunteer, as shown in Fig. 4. During the optical measurements the volunteer was asked to use a finger to support the cheek from the outside for easy control of the probe pressure and to close the mouth to maintain a relatively constant probe temperature through the study. Room lights were dimmed to very low level during the measurements to minimize the background light. Reflectance measurements were taken from each volunteer at multiple pressure levels from 0.5 ± 0.5 psi up to 9.5 ± 0.5 psi. Prior to the reflectance measurements a test run was conducted in which each volunteer was trained on how to hold the probe, read the pressure readings on the laptop screen, and maintain the probe pressure within the preset range.

Fig. 4 Photograph of DRS measurement from the left cheek of a volunteer.

At each pressure level 10 pairs of DRS and SC spectra were acquired sequentially at a 1-2 second interval. The first measurement started immediately after the desired probe pressure was reached and best effort was made

to maintain the pressure at the desired value during the 10 scans. The probe pressure at each valid scan was recorded. In order to ensure that all measurements were made from the same tissue site, there was no break for the subject during the whole study. Measurements stopped at a pressure level that the volunteer started to feel uncomfortable, resulting in different ranges of pressure levels from 0.5 ± 0.5psi to 9.5 ± 0.5psi. Table 2 summarizes the optical measurements that have been made on the left cheek from each of the 7 volunteers.

Table 2. Summary of the DRS measurements on the left cheek of the 7 volunteers at various pressure levels.

Preset Pressure (± 0.5psi)	Vol 2	Vol 3	Vol 4	Vol 5	Vol 6	Vol 7	Vol 8
0.5 psi	x	x	x	x	x	x	x
1.5 psi	x	x	x	x	x	x	x
2.5 psi	x	x	x	x	x	x	x
3.5 psi	x		x	x	x	x	x
4.5 psi	x		x	x	x	x	x
5.5 psi	x		x	x	x	x	
6.5 psi	x		x	x	x	x	
7.5 psi	x		x	x	x	x	
8.5 psi			x	x	x		
9.5 psi			x	x	x		

The DRS spectra measured from the mucosal tissues of the volunteers were calibrated (divided point-by-point) using the SC spectra collected concurrently. The self-calibrated tissue spectra and the spectrum of the best reference phantom (#7) in Table 1 (the one that gave the lowest errors) were used to extract the tissue μ_a and μ_s' spectra, following the procedures reported by Yu et al. [54]. From the extracted tissue μ_a spectrum, the HbO2 and Hb concentrations, total hemoglobin (THb) and oxygenation (SO_2) were calculated using the Beer-Lambert law (or Beer's law).

B. Constant probe pressure

In order to understand how the tissue parameters (THb, SO_2 and $< \mu_s'(\lambda) >$) of the oral mucosa respond to constant probe pressure, 100 DRS spectra have also been collected continuously from the right cheek of volunteers 2-8 under a constant probe pressure of 1-2 psi. Again, the volunteers were asked to hold the probe and maintain the preset probe pressure.

3. Experimental results

3.1. Phantom experiment

The self-calibrated phantom DRS spectra have been analyzed using the Monte Carlo inverse model of reflectance with each of the 14 phantoms as a reference. Figure 5 shows the extracted v.s. expected wavelength averaged μ_a and μ_s' as well as the THb calculated from the absorption spectra $(\mu_a(\lambda))$. The errorbars in the plots were due to the different reference phantoms. A mean error of 1.4 ± 0.5%, 6.8 ± 1.7% and 1.2 ± 1.6% were calculated for $< \mu_a(\lambda) >$, $< \mu_s'(\lambda) >$ and THb, respectively.

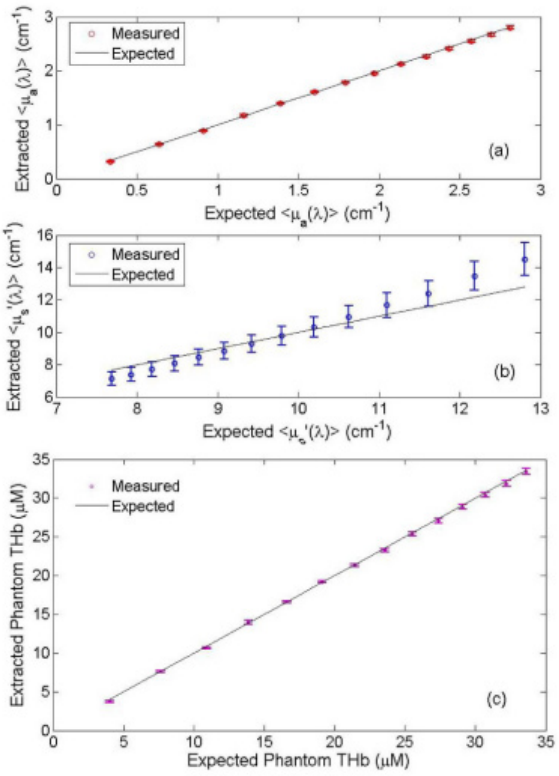

Fig. 5 Extracted v.s. expected phantom mean (a) μ_a; (b) μ_s' and (c) THb. The errorbars were resulted from different phantom for reference.

3.2. Pressure sensor characterization

Figure 6(a) shows a typical interferogram of the smart probe under room pressure (P = 0 psi). An initial cavity length of 61.54 μm was calculated from the interferogram. Figure 6(b) shows the measured air cavity length of the pressure sensor as a function of the applied nitrogen pressure. A pressure sensitivity of 218 nm/psi was determined from the linear fit. A fluctuation of ~50 nm from the expected L-P curve indicates that the uncertainty of this sensor is around 0.25 psi within 0-8 psi.

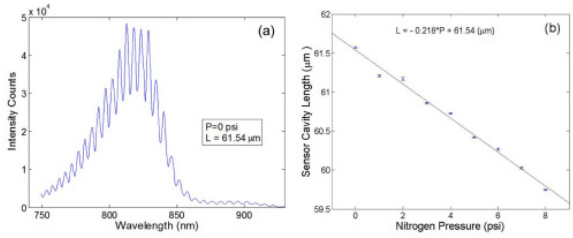

Fig. 6 Pressure sensor characterization: (a) an interferogram measured under room pressure and (b) measured cavity length as a function of the nitrogen pressure. The errorbar in (b) was obtained from the 10 repeated measurements under each pressure level.

3.3. Volunteer studies

3.3.1. Pressure control

A total of 170 pressure measurements have been taken from a finger of Vol 1 to test how good the probe pressure can be maintained on *in vivo* biological tissue. Among the 170 measurements, 50 fell within the preset pressure range of 2-3 psi. The other 120 measurements were either above or below the preset pressure range

which were mainly caused by the shaking of the hand holding the probe during the scans. In another word, it requires an average of approximately 4 scans to catch one valid measurement (within the preset range). Since each NIR scan takes less than 10 ms, one valid pressure scan can be obtained in less than 40 ms, which is fast enough for most diagnostic applications.

3.3.2. Tissue response to pressure

A. Variable probe pressure

DRS and SC spectra were obtained from the oral mucosa under increased probe pressure in 7 volunteers. Figure 7 shows the tissue HbO_2, Hb, THb, SO_2 and $< \mu_s'(\lambda) >$ measured from the left cheek of one subject (Vol 2) with a probe pressure from 0.5 ± 0.5 to 7.5 ± 0.5 psi. A general trend of decrease in HbO_2, THb, SO_2 and μ_s' and increase in Hb with probe pressure has been identified in most study subjects. The sharpest changes in all tissue parameters occur within 0-3 psi. Fluctuations in Hb and SO_2 have also been observed in most subjects. Student T-tests have been performed to investigate whether the tissue parameters measured under raised probe pressure levels (limited to 1.5, 2.5, 3.5 and 4.5 psi) are significantly different from those measured under the lowest pressure level (0.5 ± 0.5 psi). Table 3 summarizes the test results for THb, SO_2 and $< \mu_s'(\lambda) >$. In most subjects, probe pressure as low as 1.5 or 2.5 psi significantly changed ($p<0.05$) the tissue THb (except Vol 3), SO_2 (except Vol 4 and 8), and μ_s'.

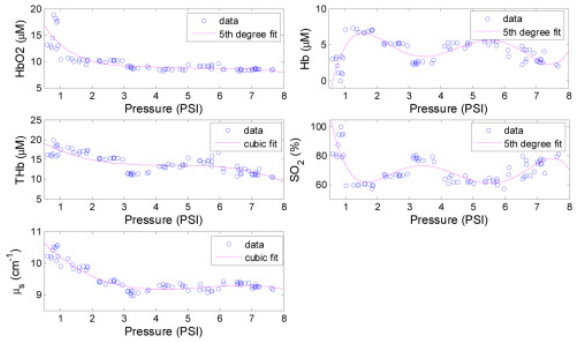

Fig. 7 Tissue HbO_2, Hb, THb, SO_2 and $< \mu_s'(\lambda) >$ measured from the left cheek of Vol 2 under increased probe pressure (8 pressure levels from 0.5 ± 0.5 psi to 7.5 ± 0.5 psi with 10 measurements under each pressure level).

Table 3. Student T-test results for THb, SO_2 and $< \mu_s'(\lambda) >$ measured with a probe pressure from 0.5 ± 0.5 psi to 4.5 ± 0.5 psi. (√: $p < 0.05$, x: $p>0.05$)

THb/SO_2/$< \mu_s'(\lambda) >$	**Vol 2**	**Vol 3**	**Vol 4**	**Vol 5**	**Vol 6**	**Vol 7**	**Vol 8**
0.5 vs. 1.5 psi	x / √ / √	x / √ / x	√ / x / √	√ / √ / √	√ / √ / √	x / x / √	x / x / √
0.5 vs. 2.5 psi	√ / √ /√	x / √ / √	√ / x / √	√ / √ / √	√ / √ / √	√ / √ / √	√ / x / √
0.5 vs. 3.5 psi	√ / √ / √		√ / √ / √	x / √ / √	√ / √ / √	x / x / √	√ / x / √
0.5 vs. 4.5 psi	√ / √ / √		√ / √ / √	x / √ / √	√ / √ / √	√ / √ / √	√ / √ / √

B. Constant probe pressure

The self-calibrated tissue DRS spectra collected from the right cheek of the 7 volunteers under a constant pressure of 1-2 psi were also analyzed to extract the tissue parameters. Figure 8 shows the typical tissue parameters extracted from the 100 repeated scans from Vol 8. A sharp drop in the HbO2, THb and SO_2 and increase in Hb in the first 10 seconds (corresponding to first 5-6 data points) have been observed. The scattering coefficients were relatively constant with less than ± 3% fluctuations (with a few outliers) for Vol 8. For all the 7 study subjects, it takes an average of 10-100 seconds for the extracted tissue parameters to stabilize upon the application of a constant pressure of 1-2 psi.

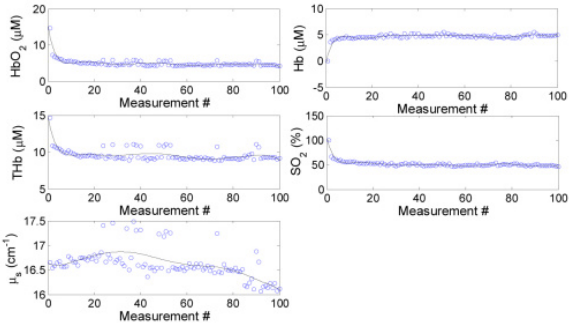

Fig. 8 Tissue parameters measured from the right cheek of Vol 8 under a constant probe pressure of 1-2 psi. The open circles represent experimental data and solid lines represent a 9th degree fit.

4. Discussions

This report describes a portable, easy-to-use and low cost smart fiber-optic sensor DRS device for noninvasive quantification of tissue optical and physiological properties *in vivo*. The device was designed to correct instrument fluctuations in real-time, eliminate operator bias, minimize tissue disturbance, and reduce the need of operator training. A series of phantom, physical and pilot clinical experiments have been conducted to investigate the performance of the device for performing tissue optical spectroscopy.

The pressure sensor is a critical component of the smart sensor system for obtaining intact tissue physiological and morphological properties. The DFPI sensor showed a high pressure sensitivity of 218 nm/psi in a pressure test setup, as shown in Fig. 6(b). A fluctuation of ~50 nm from the expected L-P curve was also observed which limited the pressure resolution to ~0.25 psi within 0-8 psi. This pressure resolution should still be sufficient for most *in vivo* DRS studies where probe pressure is mostly below 8 psi [35–37]. The major challenge encountered is the relatively large temperature sensitivity of the DFPI cavity length. The probe tip temperature is close to the body temperature (~37 °C) when it is in contact with tissue, but drops to room temperature (21-25 °C) when it is not in contact with tissue. During DRS measurement a minimum probe pressure is usually desired which means the probe should be in gentle contact with tissue, thus any hand or patient movement can cause significant fluctuation in the probe temperature. Such large fluctuation (up to 15 °C) can induce a maximum error of ± 0.5 psi in the measured pressure. This uncertainty was characterized in an independent experiment in which the probe tip was fixed in water and heated from 21 °C to 36 °C (data not shown). Therefore, a pressure range of ± 0.5 psi was used in the study for each pressure level. Reducing the sensor temperature sensitivity is desired in the future for better accuracy in measuring and control of the probe pressure.

In the volunteer study with increased probe pressure, a decrease in HbO_2, THb, SO_2 and increase in Hb with probe pressure has been observed in all subjects (Fig. 7). Fluctuations in Hb and SO_2 have also been observed for most subjects. The changes in the tissue hemoglobin concentrations and SO_2 may be attributed to the reduction in new blood supply to the region with increased probe pressure. The fluctuations in the measured Hb and SO_2 were likely caused by the return of the blood due to natural re-perfusion or shake of the hand holding the probe that changed the probe-tissue contact (over the range pressure was not recorded, but did occur). The reduced scattering $< \mu_s'(\lambda) >$ showed a general trend of decrease with probe pressure, but in one subject a small increase in scattering with pressure was recorded. The decrease in the tissue scattering disagrees with the findings in a cervical tissue study reported by Chang et al. [55] The major difference is that during this study the volunteers, except the one with increased scattering, were asked to use a finger to support the cheek against the probe, while in Chang's study the cervical tissue had no additional support in the back. This means that the oral tissues might be more compressed, resulting reduced discontinuities in the refractive indices of between scatterers, thus reduced scattering. However, further investigation is needed to better understand the scattering response to probe pressure.

The T-test results in Table 2 indicate that when a fiber-optic probe is utilized for performing DRS on oral mucosal tissue *in vivo* a probe pressure as low as 1.5 psi or less may significantly change the tissue THb, SO_2 and $< \mu_s'(\lambda) >$. This suggests that during contact DRS measurement of mucosal tissue, the probe pressure should be kept below 1.0 psi (or even lower) to minimize the disturbance to tissue physiological and morphological properties. The results in Fig. 8 indicate that even if a constant probe pressure can be maintained during DRS, it takes the tissue a certain amount of time to stabilize. This time period varies with the applied probe pressure and tissue types as well as patient movement.

Finally, the need for a three-channel spectrometer increases the cost of the smart sensor system. Even though the total cost of the smart sensor system is still under $10k and can be further reduced with mass production. More importantly, the addition of a pressure sensor and a self-calibration channel makes the otherwise unreliable and defective DRS measurements diagnostically useful. From this point of view, the benefits outweigh the costs of the system.

5. Conclusions

Diffuse reflectance spectroscopy with a fiber optic probe is a powerful tool for quantifying tissue optical and physiological properties and has found a wide range of biomedical applications, including cancer detection, therapeutic monitoring, tissue characterization, hemoglobin monitoring in critical care, etc. However, its clinical application is limited, especially in LMICs, due to the lack of real-time calibration, uncontrolled probe-tissue interface, high power consumption and cost, and demand on training. The smart sensor system is designed with state-of-the-art photonics technologies to overcome the above mentioned limitations so that it will be possible to perform accurate and reproducible DRS for rapid screening of oral and cervical cancers in LMICs. The volunteer study demonstrated the clinical usability of the device as well as the response of oral mucosal tissue to probe pressure.

Acknowledgments

This research was supported by the National Institutes of Health, National Institute of Biomedical Imaging and Bioengineering, grant No. R03EB012210.

References and links

1. O. Kujan, A. M. Glenny, R. J. Oliver, N. Thakker, and P. Sloan, "Screening programmes for the early detection and prevention of oral cancer," Cochrane Database Syst. Rev. **3**(3), CD004150 (2006).

2. R. Sankaranarayanan, K. Ramadas, G. Thomas, R. Muwonge, S. Thara, B. Mathew, B. Rajan, and Trivandrum Oral Cancer Screening Study Group, "Effect of screening on oral cancer mortality in Kerala, India: a cluster-randomised controlled trial," Lancet **365**(9475), 1927–1933 (2005).

3. Oral Cancer Foundation, Early detection is the key to beating oral cancer, Oral Cancer News, (2007)

4. CDC, *Oral Cancer Background Papers*. retrieved on September 23, 2009.

5. E. K. Adams, N. Breen, and P. J. Joski, "Impact of the National Breast and Cervical Cancer Early Detection Program on mammography and Pap test utilization among white, Hispanic, and African American women: 1996-2000," Cancer **109**(S2), 348–358 (2007).

6. D. Saslow, C. D. Runowicz, D. Solomon, A. B. Moscicki, R. A. Smith, H. J. Eyre, and C. Cohen, "American Cancer Society Guideline for the Early Detection of Cervical Neoplasia and Cancer," J. Low. Genit. Tract Dis. **7**(2), 67–86 (2003).

7. H. W. Lawson, R. Henson, J. K. Bobo, and M. K. Kaeser, "Implementing recommendations for the early detection of breast and cervical cancer among low-income women," MMWR Recomm. Rep. **49**(RR-2), 37–55 (2000).

8. J. Sherris, C. Herdman, and C. Elias, "Cervical cancer in the developing world," West. J. Med. **175**(4), 231–233 (2001).

9. M. C. Skala, G. M. Palmer, K. M. Vrotsos, A. Gendron-Fitzpatrick, and N. Ramanujam, "Comparison of a physical model and principal component analysis for the diagnosis of epithelial neoplasias in vivo using diffuse reflectance spectroscopy," Opt. Express **15**(12), 7863–7875 (2007).

10. V. T. Chang, P. S. Cartwright, S. M. Bean, G. M. Palmer, R. C. Bentley, and N. Ramanujam, "Quantitative physiology of the precancerous cervix in vivo through optical spectroscopy," Neoplasia **11**(4), 325–332 (2009).

11. M. G. Müller, T. A. Valdez, I. Georgakoudi, V. Backman, C. Fuentes, S. Kabani, N. Laver, Z. Wang, C. W. Boone, R. R. Dasari, S. M. Shapshay, and M. S. Feld, "Spectroscopic detection and evaluation of morphologic and biochemical changes in early human oral carcinoma," Cancer **97**(7), 1681–1692 (2003).

12. D. C. de Veld, M. Skurichina, M. J. Witjes, R. P. Duin, H. J. Sterenborg, and J. L. Roodenburg, "Autofluorescence and diffuse reflectance spectroscopy for oral oncology," Lasers Surg. Med. **36**(5), 356–364 (2005).

13. A. Sharwani, W. Jerjes, V. Salih, B. Swinson, I. J. Bigio, M. El-Maaytah, and C. Hopper, "Assessment of oral premalignancy using elastic scattering spectroscopy," Oral Oncol. **42**(4), 343–349 (2006).

14. N. Subhash, J. R. Mallia, S. S. Thomas, A. Mathews, P. Sebastian, and J. Madhavan, "Oral cancer detection using diffuse reflectance spectral ratio R540/R575 of oxygenated hemoglobin bands," J. Biomed. Opt. **11**(1), 014018 (2006).

15. A. Amelink, O. P. Kaspers, H. J. Sterenborg, J. E. van der Wal, J. L. Roodenburg, and M. J. Witjes, "Non-invasive measurement of the morphology and physiology of oral mucosa by use of optical spectroscopy," Oral Oncol. **44**(1), 65–71 (2008).

16. M. Rahman, P. Chaturvedi, A. M. Gillenwater, and R. Richards-Kortum, "Low-cost, multimodal, portable screening system for early detection of oral cancer," J. Biomed. Opt. **13**(3), 030502 (2008).

17. R. A. Schwarz, W. Gao, D. Daye, M. D. Williams, R. Richards-Kortum, and A. M. Gillenwater, "Autofluorescence and diffuse reflectance spectroscopy of oral epithelial tissue using a depth-sensitive fiber-optic probe," Appl. Opt. **47**(6), 825–834 (2008).

18. Y. N. Mirabal, S. K. Chang, E. N. Atkinson, A. Malpica, M. Follen, and R. Richards-Kortum, "Reflectance spectroscopy for in vivo detection of cervical precancer," J. Biomed. Opt. **7**(4), 587–594 (2002).

19. S. K. Chang, Y. N. Mirabal, E. N. Atkinson, D. Cox, A. Malpica, M. Follen, and R. Richards-Kortum, "Combined reflectance and fluorescence spectroscopy for in vivo detection of cervical pre-cancer," J. Biomed. Opt. **10**(2), 024031 (2005).

20. M. Follen, S. Crain, C. MacAulay, K. Basen-Engquist, S. B. Cantor, D. Cox, E. N. Atkinson, N. MacKinnon, M. Guillaud, and R. Richards-Kortum, "Optical technologies for cervical neoplasia: update of an NCI program project grant," Clin. Adv. Hematol. Oncol. **3**(1), 41–53 (2005).

21. N. M. Marín, A. Milbourne, H. Rhodes, T. Ehlen, D. Miller, L. Benedet, R. Richards-Kortum, and M. Follen, "Diffuse reflectance patterns in cervical spectroscopy," Gynecol. Oncol. **99**(3Suppl 1), S116–S120 (2005).

22. D. Arifler, C. MacAulay, M. Follen, and R. Richards-Kortum, "Spatially resolved reflectance spectroscopy for diagnosis of cervical precancer: Monte Carlo modeling and comparison to clinical measurements," J. Biomed. Opt. **11**(6), 064027 (2006).

23. M. Cardenas-Turanzas, J. A. Freeberg, J. L. Benedet, E. N. Atkinson, D. D. Cox, R. Richards-Kortum, C. MacAulay, M. Follen, and S. B. Cantor, "The clinical effectiveness of optical spectroscopy for the in vivo diagnosis of cervical intraepithelial neoplasia: where are we?" Gynecol. Oncol. **107**(1Suppl 1), S138–S146 (2007).

24. J. A. Freeberg, J. L. Benedet, C. MacAulay, L. A. West, and M. Follen, "The performance of fluorescence and reflectance spectroscopy for the in vivo diagnosis of cervical neoplasia; point probe versus multispectral approaches," Gynecol. Oncol. **107**(1Suppl 1), S248–S255 (2007).

25. A. Wang, V. Nammalavar, and R. Drezek, "Targeting spectral signatures of progressively dysplastic stratified epithelia using angularly variable fiber geometry in reflectance Monte Carlo simulations," J. Biomed. Opt. **12**(4), 044012 (2007).

26. D. Arifler, R. A. Schwarz, S. K. Chang, and R. Richards-Kortum, "Reflectance spectroscopy for diagnosis of epithelial precancer: model-based analysis of fiber-optic probe designs to resolve spectral information from epithelium and stroma," Appl. Opt. **44**(20), 4291–4305 (2005).

27. P. M. Lane, T. Gilhuly, P. Whitehead, H. Zeng, C. F. Poh, S. Ng, P. M. Williams, L. Zhang, M. P. Rosin, and C. E. MacAulay, "Simple device for the direct visualization of oral-cavity tissue fluorescence," J. Biomed. Opt. **11**(2), 024006 (2006).

28. I. Pavlova, C. R. Weber, R. A. Schwarz, M. D. Williams, A. M. Gillenwater, and R. Richards-Kortum, "Fluorescence spectroscopy of oral tissue: Monte Carlo modeling with site-specific tissue properties," J. Biomed. Opt. **14**(1), 014009 (2009).

29. R. Hasina and M. W. Lingen, "Angiogenesis in oral cancer," J. Dent. Educ. **65**(11), 1282–1290 (2001).

30. I. Georgakoudi, E. E. Sheets, M. G. Müller, V. Backman, C. P. Crum, K. Badizadegan, R. R. Dasari, and M. S. Feld, "Trimodal spectroscopy for the detection and characterization of cervical precancers in vivo," Am. J. Obstet. Gynecol. **186**(3), 374–382 (2002).

31. Q. Liu and N. Ramanujam, "Sequential estimation of optical properties of a two-layered epithelial tissue model from depth-resolved ultraviolet-visible diffuse reflectance spectra," Appl. Opt. **45**(19), 4776–4790 (2006).

32. C. Zhu, G. M. Palmer, T. M. Breslin, F. Xu, and N. Ramanujam, "Use of a multiseparation fiber optic probe for the optical diagnosis of breast cancer," J. Biomed. Opt. **10**(2), 024032 (2005).

33. G. M. Palmer and N. Ramanujam, "Monte Carlo-based inverse model for calculating tissue optical properties. Part I: Theory and validation on synthetic phantoms," Appl. Opt. **45**(5), 1062–1071 (2006).

34. U. Utzinger and R. R. Richards-Kortum, "Fiber optic probes for biomedical optical spectroscopy," J. Biomed. Opt. **8**(1), 121–147 (2003).

35. E. K. Chan, B. Sorg, D. Protsenko, M. O'Neil, M. Motamedi, and A. J. Welch, "Effects of compression on soft tissue optical properties," IEEE J. Sel. Top Quantum Electron. **2**(4), 943–950 (1996).

36. R. Reif, M. S. Amorosino, K. W. Calabro, O. A'Amar, S. K. Singh, and I. J. Bigio, "Analysis of changes in reflectance measurements on biological tissues subjected to different probe pressures," J. Biomed. Opt. **13**(1), 010502 (2008).

37. Y. Ti and W. C. Lin, "Effects of probe contact pressure on in vivo optical spectroscopy," Opt. Express **16**(6), 4250–4262 (2008).

38. A. Nath, K. Rivoire, S. Chang, D. Cox, E. N. Atkinson, M. Follen, and R. Richards-Kortum, "Effect of probe pressure on cervical fluorescence spectroscopy measurements," J. Biomed. Opt. **9**(3), 523–533 (2004).

39. K. Rivoire, A. Nath, D. Cox, E. N. Atkinson, R. Richards-Kortum, and M. Follen, "The effects of repeated spectroscopic pressure measurements on fluorescence intensity in the cervix," Am. J. Obstet. Gynecol. **191**(5), 1606–1617 (2004).

40. H. Shangguan, S. A. Prahl, S. L. Jacques, and L. W. Casperson, "Pressure effects on soft tissues monitored by changes in tissue," Proc. SPIE **3254**, 366 (1998).

41. J. A. D. Atencio, E. E. O. Guillén, S. V. y. Montiel, M. C. Rodríguez, J. C. Ramos, J. L. Gutiérrez, and F. Martínez, "Influence of probe pressure on human skin diffuse reflectance spectroscopy measurements," Opt. Mem. Neural. Networks **18**(1), 6–14 (2009).

42. W. Chen, R. Liu, K. Xu, and R. K. Wang, "Influence of contact state on NIR diffuse reflectance spectroscopy in vivo," J. Phys. D Appl. Phys. **38**(15), 2691–2695 (2005).

43. S. Ruderman, A. J. Gomes, V. Stoyneva, J. D. Rogers, A. J. Fought, B. D. Jovanovic, and V. Backman, "Analysis of pressure, angle and temporal effects on tissue optical properties from polarization-gated spectroscopic probe measurements," Biomed. Opt. Express **1**(2), 489–499 (2010).

44. A. Kienle, L. Lilge, M. S. Patterson, R. Hibst, R. Steiner, and B. C. Wilson, "Spatially resolved absolute diffuse reflectance measurements for noninvasive determination of the optical scattering and absorption coefficients of biological tissue," Appl. Opt. **35**(13), 2304–2314 (1996).

45. S. C. Gebhart, R. C. Thompson, and A. Mahadevan-Jansen, "Liquid-crystal tunable filter spectral imaging for brain tumor demarcation," Appl. Opt. **46**(10), 1896–1910 (2007).

46. S. F. Bish, N. Rajaram, B. Nichols, and J. W. Tunnell, "Development of a noncontact diffuse optical spectroscopy probe for measuring tissue optical properties," J. Biomed. Opt. **16**(12), 120505 (2011).

47. D. J. Cuccia, F. Bevilacqua, A. J. Durkin, F. R. Ayers, and B. J. Tromberg, "Quantitation and mapping of tissue optical properties using modulated imaging," J. Biomed. Opt. **14**(2), 024012 (2009).

48. M. G. Nichols, E. L. Hull, and T. H. Foster, "Design and testing of a white-light, steady-state diffuse reflectance spectrometer for determination of optical properties of highly scattering systems," Appl. Opt. **36**(1), 93–104 (1997).

49. N. M. Marín, N. MacKinnon, C. MacAulay, S. K. Chang, E. N. Atkinson, D. Cox, D. Serachitopol, B. Pikkula, M. Follen, and R. Richards-Kortum, "Calibration standards for multicenter clinical trials of fluorescence spectroscopy for in vivo diagnosis," J. Biomed. Opt. **11**(1), 014010 (2006).

50. G. Zonios, L. T. Perelman, V. Backman, R. Manoharan, M. Fitzmaurice, J. Van Dam, and M. S. Feld, "Diffuse reflectance spectroscopy of human adenomatous colon polyps in vivo," Appl. Opt. **38**(31), 6628–6637 (1999).

51. U. Utzinger, M. Brewer, E. Silva, D. Gershenson, R. C. Blast Jr, M. Follen, and R. Richards-Kortum, "Reflectance spectroscopy for in vivo characterization of ovarian tissue," Lasers Surg. Med. **28**(1), 56–66 (2001).

52. P. Thueler, I. Charvet, F. Bevilacqua, M. St. Ghislain, G. Ory, P. Marquet, P. Meda, B. Vermeulen, and C. Depeursinge, "In vivo endoscopic tissue diagnostics based on spectroscopic absorption, scattering, and phase function properties," J. Biomed. Opt. **8**(3), 495–503 (2003).

53. B. Yu, H. Fu, T. Bydlon, J. E. Bender, and N. Ramanujam, "Diffuse reflectance spectroscopy with a self-calibrating fiber optic probe," Opt. Lett. **33**(16), 1783–1785 (2008).

54. B. Yu, H. L. Fu, and N. Ramanujam, "Instrument independent diffuse reflectance spectroscopy," J. Biomed. Opt. **16**(1), 011010 (2011).

55. V. T.-C. Chang, D. Merisier, B. Yu, D. K. Walmer, and N. Ramanujam, "Towards a field-compatible optical spectroscopic device for cervical cancer screening in resource-limited settings: effects of calibration and pressure," Opt. Express **19**(19), 17908–17924 (2011).

56. B. Yu, D. W. Kim, J. Deng, H. Xiao, and A. Wang, "Fiber Fabry-Perot sensors for detection of partial discharges in power transformers," Appl. Opt. **42**(16), 3241–3250 (2003).

57. B. Yu, A. Wang, G. Pickrell, and J. Xu, "Tunable-optical-filter-based white-light interferometry for sensing," Opt. Lett. **30**(12), 1452–1454 (2005).

58. J. Xu, G. R. Pickrell, B. Yu, M. Han, Y. Zhu, X. Wang, K. L. Cooper, and A. Wang, "Epoxy-free high temperature fiber optic pressure sensors for gas turbine engine applications," Proc. SPIE **5590**, 1 (2004).

59. B. Yu, D. W. Kim, J. Deng, H. Xiao, and A. Wang, "Fiber Fabry-Perot Sensors for Detection of Partial Discharges in Power Transformers," Appl. Opt. **42**(16), 3241–3250 (2003).

60. B. Qi, G. R. Pickrell, J. Xu, P. Zhang, Y. Duan, W. Peng, Z. Huo, H. Xiao, R. G. May, and A. Wang, "Novel data processing techniques for dispersive white light interferometer," Opt. Eng. **42**(11), 3165–3171 (2003).